Investigating the Effect of Lenses in a Long Interferometer Arm

LIGO P1400191-v1

Brian Dawes*
Mentor: Sheila Dwyer†

September 26, 2014

Abstract

Current gravitational wave interferometers are approaching fundamental limits to their sensitivity. In order to build more sensitive gravitational wave detectors, significant changes must be made to the current advanced LIGO design. One simple way to increase the sensitivity of a next generation detector is to increase the length of its arms. However as the length of the arm increases, the beam width also expands. A larger beam would require larger optics and a larger beam tube, both of which are costly and can be difficult to manufacture. In this paper, I examine the possibility of placing lenses within the beam tube of a 40km long interferometer in order to maintain a narrow beam throughout the entire detector arm. I first examine different configurations of lenses that could achieve this and then investigate how motion of the lenses can add noise to the detector to propose limits on the required seismic isolation of the lenses. I also show these lenses can be created from flat pieces of fused silica through thermal lensing and thermal expansion effects.

1 Introduction

Current gravitational wave interferometers are approaching fundamental limits to their sensitivity. Several design have been proposed for next generation gravitational wave interferometers to increase their sensitivity. One idea is to simply increase the size of the detector, for example by a factor of 10. Naively, increasing the length of the detector by a factor of 10 will also increase its sensitivity by a factor of 10. Laser interferometers detect strains which are commonly represented as:

$$h = \frac{\Delta L}{L} \tag{1}$$

*Columbia University
†LIGO Hanford Observatory

where L is the unstrained length of the detector arms and ΔL is the change in the length of the arms when the strain is present. A passing gravitational wave produces a strain which does not depend on the length of the detector. However, displacement noises produce a ΔL independent of the length of the detector. This means that the strain noise due to displacement noises is dependent on the detector's length. If L is increased by a factor of 10, the corresponding displacement noise strains will be 10 times smaller due to the increased value of L. This allows the detector to be 10 times more sensitive to gravitational waves at frequencies where displacement noises are the limiting sources of noise. Viewing the detector in terms of strains, it is not the signal that increases but rather the noise that decreases. However, this is not a complete picture. There are several other factors that must be considered to fully understand the effect that increasing the length of the detector will have.

The aLIGO detector does not contain any optics between the Input Test Mass (ITM) and the End Test Mass (ETM), which are reflective surfaces which form resonators in the detector arms to magnify the power in the detector[1]. If we increase the distance between the ITM and ETM without adding any additional optics, the beam will diverge and become become very wide. Running a detector with a wide beam is theoretically possible, but it is not very practical as it would require increasing the width of the beam tube for the entire length of the detector and increasing the size of the optics, both of which are costly and can be difficult to manufacture. In order for the beam to remain narrow over a longer distance, additional lenses can be added throughout the beam tube. However, these optics can also introduce additional noise to the detector through misalignments and thermal noise. In this paper, we examine configurations of lenses that could be used to propagate a narrow beam along the 40 km arm. We then calculate the noise introduced by motion of these lenses to determine what level of seismic isolation is required to prevent this noise from being a limiting factor for the detector. Finally, we study the thermal lensing effect in the lenses as this will significantly change the optical properties of the lenses.

2 Choosing a Cavity

In order to increase their sensitivity, the LIGO gravitational wave interferometers allow light to resonate in the arm cavities which amplifies the power of the light contained within the cavity. To achieve this, the optics must be configured such that the light constructively interferes with itself after completing a full path through the beam tube. In this section, we will first discuss the mathematical requirements for a stable resonator. Next, we will present a method which can be used to find symmetric cavities containing lenses that can propagate a beam 40 km without significant divergence of the beam.

Optical Element	ABCD Matrix
Propagation a distance L through a vacuum	$\begin{bmatrix} 1 & L \\ 0 & 1 \end{bmatrix}$
Propagation through a lens with focal length f	$\begin{bmatrix} 1 & 0 \\ -\frac{1}{f} & 1 \end{bmatrix}$
Propagation through a mirror with radius of curvature R	$\begin{bmatrix} 1 & 0 \\ -\frac{2}{R} & 1 \end{bmatrix}$

Table 1: ABCD matrices for several common optical elements

2.1 Ray Transfer Matrices

To calculate how a laser is affected by the optics along its path, we can use ray transfer matrices, more commonly known as ABCD matrices. The ability of a cavity to form a resonator can be deduced solely from its ABCD matrix. The following section is adapted from chapters 20-22 of A.E. Siegman's *Lasers*, which describe ABCD matrices and their applications to resonators [2].

A Gaussian beam of light can be represented by a complex parameter q, defined as:

$$\frac{1}{q} \equiv \frac{1}{R} - i\frac{\lambda}{\pi w^2} \tag{2}$$

where R is the radius of curvature of the wavefront, λ is the wavelength of the light, and w is the beam width. An optical element is modeled by a 2x2 matrix, often referred to as an ABCD matrix as the matrix elements are conventionally labeled as such:

$$\begin{bmatrix} A & B \\ C & D \end{bmatrix} \tag{3}$$

The ABCD matrices for a few common optical elements are shown in Table 1.

ABCD matrices allow us to easily calculate how an optical element effects a Gaussian beam. When a beam q_1 propagates through an optical element, the output beam q_2 is related to the input beam by:

$$q_2 = \frac{Aq_1 + B}{Cq_1 + D} \tag{4}$$

where A, B, C, and D refer to the elements of the optic's ABCD matrix.

ABCD matrices also allow us to simplify complicated beam paths using matrix multiplication. A beam path containing multiple elements can be described by the product of the ABCD matrices of the various optical elements in the path. Note that matrix multiplication is not commutative in general so one must multiply the matrices in the order the beam passes through each element with the first element on the right and the last element on the left.

In order for a cavity to resonate, the q parameter of the beam must remain the same after one complete round trip through the cavity. If we know the ABCD matrix for a cavity, we can solve for the q values which satisfy this self-consistency criteria, known as the eigenmodes of the cavity. Doing so will lead to a quadratic with solutions:

$$q_{1,2} = \frac{A - D \pm \sqrt{(D-A)^2 + 4BC}}{2C} \tag{5}$$

Generally only one of these solutions will correspond to a physical, confined solution which falls off at a large distance from the axis of the resonator.

We also would like to have a stable resonator, in the sense that a small perturbation to the input beam will decrease after completing a round trip through the cavity. In other words, if a beam $q + \Delta q_1$ is sent into the resonator, where q is the eigenmode of our cavity and Δq_1 is a small perturbation, we want the output of the beam after one full roundtrip through the cavity to be $q + \Delta q_2$ with $|\Delta q_2| < |\Delta q_1|$. This ensures that a small fluctuation in the input will cancel out after looping through the cavity multiple times, leaving only the cavity's eigenmode. This criteria can be quantified by an m parameter for the cavity, defined as:

$$m \equiv \frac{A + D}{2} \tag{6}$$

which is simply half the trace of the cavity's ABCD matrix. The requirement that the resonator is stable under small perturbations in q is equivalent to the requirement:

$$-1 \leq m \leq 1 \tag{7}$$

2.2 Transverse Mode Spacing

In order to find a suitable cavity, we must also consider the transverse mode spacing. Each cavity permits several transverse electro-magnetic (TEM) modes, conventionally labeled TEM_{mn} where m and n run from 0 to ∞. Gravitational wave interferometers are designed such that the lowest order mode, TEM_{00}, is resonant in the arm cavities and the next several higher order modes are not resonant. We will restrict ourselves to only considering configurations in which the first 10 higher order modes are not resonant.

The Gouy phase shift of the cavity, an additional phase which Gaussian beams acquire as they propagate, allows us to ensure that these higher order modes are not resonant. If the Gouy phase of the round trip path through a cavity is η, a TEM_{mn} beam that completes a round trip path through the cavity will acquire an additional phase shift $(m + n + 1)\eta$. If the arm cavity is locked to the TEM_{00} mode, the TEM_{mn} mode will only be resonant if:

$$(m + n)\eta = 2\pi k \tag{8}$$

where k is an integer. We can use this to define the transverse mode spacing S of the cavity:

$$S = \frac{\eta}{2\pi} \tag{9}$$

The transverse mode spacing of the cavity tells us which modes will be resonant when the TEM_{00} mode is at resonance. If $(m+n)S$ is an integer, then the TEM_{mn} has the same resonant condition as the TEM_{00} mode. For this reason, an ideal cavity would have an irrational S so that no higher order modes are resonant. However, resonances are not infinitely narrow so modes where $(m+n)S$ is close to an integer will still resonate.

In order to achieve a small spot size on our optics, it is logical to consider a symmetric cavity as any deviation from the perfectly symmetric case will decrease the spot size on one optic but increase the spot size on another. We will consider a cavity of length L with ITM and ETM mirrors with the same radius of curvature R. $N-1$ lenses are evenly spaced within the cavity separating the cavity into N smaller cavities, each with length L/N. The focal lengths of the lenses are $R/2$ so that each lens has the same ABCD matrix as the two mirrors. We can solve for R in terms of L, N, and S. First we can relate the Rayleigh range z_R of the cavity with η or S[2]:

$$\frac{\eta}{4N} = \arctan\left(\frac{L}{2Nz_R}\right) = \frac{\pi S}{2N} \tag{10}$$

$$z_R = \frac{L}{2N\tan(\pi S/2N)} \tag{11}$$

Note that η and S will always be positive and from Equation 10 we see that $S < N$ as well.

Using z_R, we can solve for the radius of curvature of the wavefront at the mirrors, which will be equal to the radius of curvature of the mirrors if the cavity is properly mode matched[2]:

$$R = \frac{L}{2N} + \frac{2Nz_R^2}{L} = \frac{L}{2N}\csc^2(\pi S/2N) \tag{12}$$

We can also solve for the spot size at our optics, w[2]:

$$w = w_0\sqrt{1+\left(\frac{L}{2Nz_R}\right)^2} = \sqrt{\frac{\lambda L}{\pi N}\csc(\pi S/N)} \tag{13}$$

where $w_0 = \sqrt{\lambda z_R/\pi}$ is the waist spot size and λ is the wavelength of the light.

Examining Equations 12 and 13, we see that both R and w vary directly with L and inversely with N. If we want to find the number of lenses required to achieve a specific radius of curvature or spot size, we can use these relations to find the required number of lenses for a certain arm length. Note that since the csc terms in Equations 12 and 13 have different periods, R and w do not achieve their minima at the same values of S and so optimizing for both of these parameters is not entirely straightforward.

2.3 Selecting a Configuration

We want to choose a stable symmetric lens configuration in which the first 10 higher order modes are not resonant. We also want a maximum spot size of

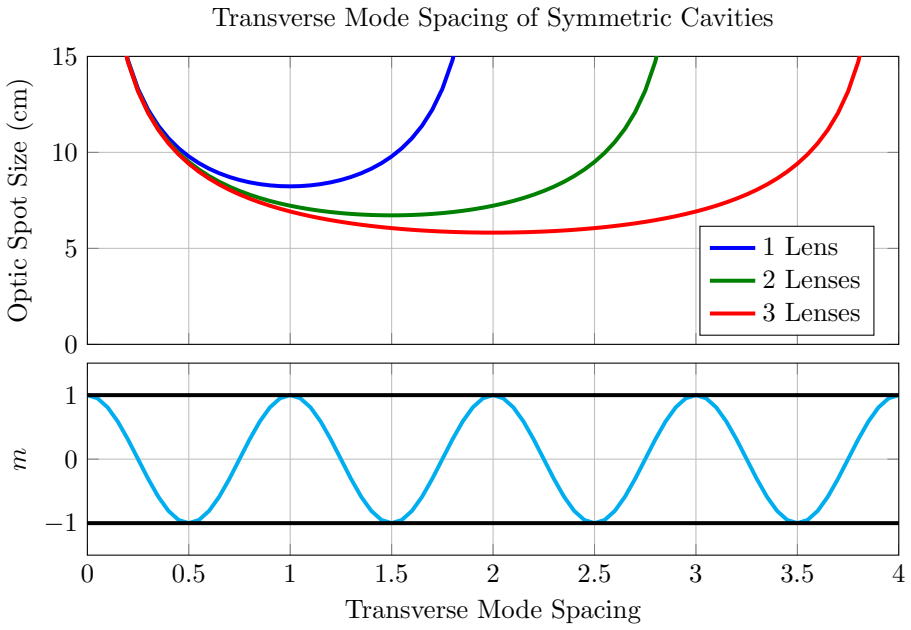

Figure 1: The effects of transverse mode spacing on spot size and resonator stability. The top figure shows the spot size on the optic as a function of the transverse mode spacing in 1, 2, or 3 lens cavities using 1064 nm light. The bottom figure shows the m parameter of the symmetric cavities as a function of the transverse mode spacing. Note that this is the same for all symmetric cavities regardless of wavelength or number of lenses.

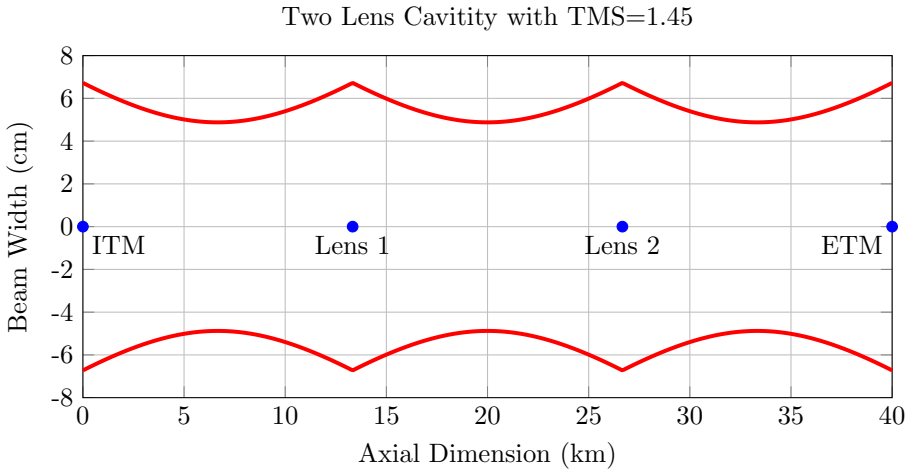

Figure 2: The beam path through the selected lens configuration with a transverse mode spacing of 1.45.

around 6 cm which is the largest spot size on the aLIGO test mass mirrors[1]. The top plot of Figure 1 shows the effect the transverse mode spacing and number of lenses have on the optic spot size. With only one lens, the minimum spot size is 8.2 cm, which is significantly larger than the aLIGO spot size. With two lenses, the minimum is 6.7 cm which is only slightly bigger than the aLIGO ETM spot size and should be possible. Using three lenses, we can further decrease the spot size to 5.8 cm which is definitely small enough.

Either a two lens or a three lens cavity should be suitable for our interferometer. Since each additional lens will introduce more noise and increase the complexity of our interferometer design, we prefer a two lens configuration. The minimum spot size for a two lens cavity occurs at $S = 1.5$. This minimum will not work as at $S = 1.5$ the second order modes will be resonant. Additionally, at $S = 1.5$, $m = -1$ which means the detector is nearly unstable and any imperfections in the cavity can push the m factor below -1 into an unstable region. However, we can simply choose $S = 1.45$, which is only slightly off from the minimum spot size and thus also has a 6.7 cm spot size. With $S = 1.45$, the first resonant higher order mode is the 20^{th}. From Equation 12, we calculate a mirror radius of curvature of 14 070 m and a corresponding lens focal length of 7035 m. The resulting beam path is plotted in Figure 2.

3 Misalignment Noise

3.1 Modal Model of Misalignments

In an ideal experiment our lenses and mirrors would be completely isolated from any outside disturbances besides the strain of a passing gravitational wave

but in reality our detector is subject to various sources of noise which can cause the optics to shift out of alignment. We must check how these small misalignments will affect the sensitivity of our hypothetical long detector. A formalism for modeling the effects of optical misalignment has been created by Hefetz et al.[3]. Using the paraxial approximation, we can represent a light beam passing through the cavity as a superposition of Hermite-Gaussian beams. These beams are also known as transverse electromagnetic (TEM) modes. These modes can be labeled as $\mathrm{TEM_{ij}}$ modes, where i and j run from 0 to ∞. These modes form a basis for the allowed electric fields of our detector. If our detector is perfectly aligned, it will consist of only a $\mathrm{TEM_{00}}$ beam. When this beam passes through a misaligned optic, some of the power of the $\mathrm{TEM_{00}}$ mode will be transferred into higher order modes. These higher order modes generally do not resonate in the same cavities as the $\mathrm{TEM_{00}}$ mode, so any power transferred to a higher order mode can be considered lost power. A misalignment can be represented as an operator which acts on the basis of TEM modes. This formalism allows us to see the effects of misalignment through linear algebra so we do not have to re-solve the wave equation with our misaligned optic.

For most purposes, only the lowest order modes, $\mathrm{TEM_{00}}$, $\mathrm{TEM_{10}}$, and $\mathrm{TEM_{01}}$, need to be considered. Misalignments in the $\mathrm{TEM_{10}}$ and $\mathrm{TEM_{01}}$ modes are caused by motion in independent directions so we can eliminate another dimension by only considering motion in one direction at a time. We thus only need to consider the $\mathrm{TEM_{00}}$ and $\mathrm{TEM_{10}}$ modes. An electric field $\mathbf{E}$ can be expressed in vector form as:

$$\mathbf{E} = \begin{bmatrix} E_{00} \\ E_{10} \end{bmatrix} \tag{14}$$

where E_{00} and E_{10} are the components of $\mathbf{E}$ in the $\mathrm{TEM_{00}}$ and $\mathrm{TEM_{10}}$ modes respectively. Misaligned optics can be represented as matrices which act on these electric field vectors.

Hefetz et al. list several operators for different types of misalignments. The first is the effect of a misaligned lens. If a lens is rotated about the y-axis by a small angle θ_x, the beam is translated by:

$$\Delta x \approx \theta_x (1 - \frac{1}{n}) d \tag{15}$$

where n is the index of refraction of the lens and d is the thickness of the lens. The effects of this translation can be approximated to second order by the matrix:

$$\begin{bmatrix} 1 - \frac{|t|^2}{2w^2}(\Delta x)^2 & \frac{it^*}{w}\Delta x \\ \frac{it}{w}\Delta x & 1 - \frac{|t|^2}{2w^2}(\Delta x)^2 \end{bmatrix} \tag{16}$$

$$t = i - \frac{\pi w^2}{\lambda R} \tag{17}$$

where i is the imaginary unit, w and R are the beam width and radius of curvature at the lens, and λ is the wavelength of the light. This operator is known as the lateral shift operator, as it corresponds to a lateral shift of the beam.

We would also like to see the effect a misaligned mirror will have on the beam. When a mirror is rotated by a small angle θ_x about the y axis, the misalignment can be approximated to second order by the following matrix:

$$\begin{bmatrix} 1 - 2\left(\theta_x \frac{\pi w}{\lambda}\right)^2 & -2i\theta_x \frac{\pi w}{\lambda} \\ -2i\theta_x \frac{\pi w}{\lambda} & 1 - 2\left(\theta_x \frac{\pi w}{\lambda}\right)^2 \end{bmatrix} \tag{18}$$

This operator is known as the tilt operator.

One last effect to consider is the motion of the lens in the plane transverse to the direction of beam propagation. Hefetz et al. do not calculate this effect, however it can be deduced from the tilt operator as transverse motion of a lens also deflects the beam from the optical axis. From basic ray optics and geometry, a mirror rotated by θ_x causes a deflection of $2\theta_x$. A beam passing through a distance Δx from the center of a lens of focal length f is deflected by $\arctan(\Delta x/f) \approx \Delta x/f$. Comparing these deflection, we can see that the misalignment matrix for the lens is:

$$\begin{bmatrix} 1 - \frac{1}{2}\left(\frac{\pi w \Delta x}{\lambda f}\right)^2 & -i\frac{\pi w \Delta x}{\lambda f} \\ -i\frac{\pi w \Delta x}{\lambda f} & 1 - \frac{1}{2}\left(\frac{\pi w \Delta x}{\lambda f}\right)^2 \end{bmatrix} \tag{19}$$

If we assume that our initial electric field is purely in the TEM_{00} mode then we only care about the first column of these matrices, which describes how the TEM_{00} mode transforms into the TEM_{10} mode. To calculate the power lost in the TEM_{00} mode we can either look at the element in the first row of this column, which measures the relative amplitude of the electric field that remains in the TEM_{00} mode, or we can look at the element in the second row, which shows the amplitude of the relative electric field that is produced in the TEM_{10} mode. To get the relative power in these modes, we can look at the magnitude squared of these matrix elements. Due to energy conservation, the sum of the magnitude squared of these two values should be equal to 1. Our matrices agree with this requirement to second order.

Using our above matrices, we can see that the fractional power loss due to a lens rotated θ_l about the y axis is:

$$P_l = (\frac{1}{w^2} + \frac{\pi^2 w^2}{\lambda^2 R^2})(1 - 1/n)^2 d^2 \theta_l^2 \tag{20}$$

Similarly, a mirror rotated θ_m about the y axis causes a fractional power loss of:

$$P_m = 4\frac{\pi^2 w^2}{\lambda^2}\theta_m^2 \tag{21}$$

And finally, a beam passing Δx from the center of a lens of focal length f causes a fractional power loss:

$$P_t = \left(\frac{\pi w \Delta x}{\lambda f}\right)^2 \tag{22}$$

In addition to the misalignment matrices, we also have a propagator matrix which describes the propagation of a beam in vacuum:

$$\begin{bmatrix} e^{i\eta} & 0 \\ 0 & e^{2i\eta} \end{bmatrix} \tag{23}$$

where η is the Guoy phase shift across the distance propagated.

In this modal system, we can calculate the round trip propagation matrix P_{rt} as:

$$P_{rt} = (-r_1)(-r_2)t_l^4 M_1 P L_1 P L_2 P M_2 P L_2 P L_1 P \tag{24}$$

where r_1, r_2 are the reflection coefficients of the mirrors, t_l is the transmission coefficient of the lenses, M_1, M_2 are the mirror misalignment matrices, L_1, L_2 are the lens misalignment matrices, and P is the propagator between each pair of elements. We can then solve for the steady-state field inside the arm using the cavity equation:

$$E_{ins} = t_1(I - P_{rt})^{-1} E_0 \tag{25}$$

where t_1 is the transmission coefficient of the first mirror, I is the identity matrix, and E_0 is the input electric field[3].

3.2 Seismic Motion Limits

Seismic motion can cause the lenses to move slightly which will cause the beam to fall off the center of the lenses. If the beam passes through a lens off-center, the optical path length will change which registers as a signal in the detector readout. There are two ways transverse displacement of the optics can cause an optical path difference. Convex lenses have maximum thickness at their centers and become thinner by their edges. When the beam is off-center, the beam will travel through the lens for a shorter distance than normal and stay in vacuum for slightly longer. Since the lens and the vacuum have different indices of refraction the beam will have a different phase than the centered beam. Once the beam passes through the optic, it will also be deflected at an angle from the optical axis of the detector. The optical path length increases as the beam is no longer traveling on a straight line through the detector. Both of these effects are shown in Figure 4.

If the beam only oscillates a small distance around the center of the optic, both effects depend quadratically on the motion of the optic and are negligible. However, if the beam is already misaligned, we will also see a noise term which depends on the product of the initial misalignment and the periodic displacement due to seismic noise.

For seismic motion above 0.5 Hz, LIGO uses a system of multiple suspensions to reduce the motion of optics. Depending on the sensitivity of the optic, three or four stages of suspension are used. The transfer functions for transverse motion of a quad test mass suspension and a beam splitter triple suspension hanging from wires are shown in Figure 3. Ground motion in both the horizontal and vertical transverse directions are similar but the isolation for vertical motion

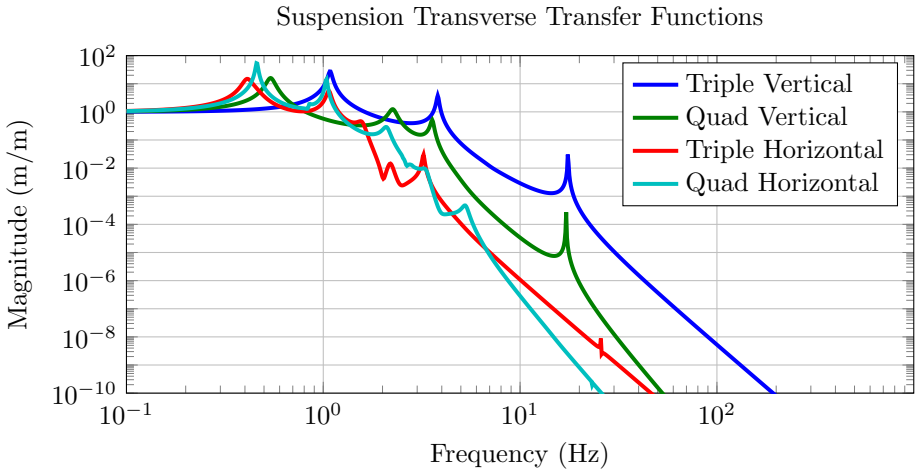

Figure 3: Transfer functions for transverse motion of the LIGO triple and quad suspension systems. These transfer functions describe coupling from the support to the optic. Further isolation from ground motion can be achieved through an internal seismic isolation (ISI) system, although this would be expensive. Both suspension systems have significantly higher transfer functions for vertical motion at frequencies above 2 Hz. At higher frequencies, the quad suspension system isolates significantly better than the triple suspension system.

is significantly higher for both the triple and quad suspensions, indicating that vertical motion will set our limit for seismic isolation. Since ground motion decreases and seismic isolation increases at higher frequencies, the seismic noise is most significant at lower frequencies. To find our limit for seismic isolation, we thus only need to examine the noise at the lowest frequency we would like to be sensitive to, 10 Hz.

3.2.1 Lens Thickness

The left image of Figure 4 shows an off-centered beam traveling through a lens for a shorter distance than a centered beam. Due to the index of refraction difference between the lens and the vacuum, this creates an optic path length difference. Compared to a centered beam, a beam that is displaced a distance x from the center of the optic will travel through the lens a distance z less on each side:

$$z = R\left(1 - \sqrt{1 - \frac{x^2}{R^2}}\right) \approx \frac{x^2}{2R} \tag{26}$$

where R is the radius of curvature of the lens.

If the beam is then displaced an additional distance δx for a total displace-

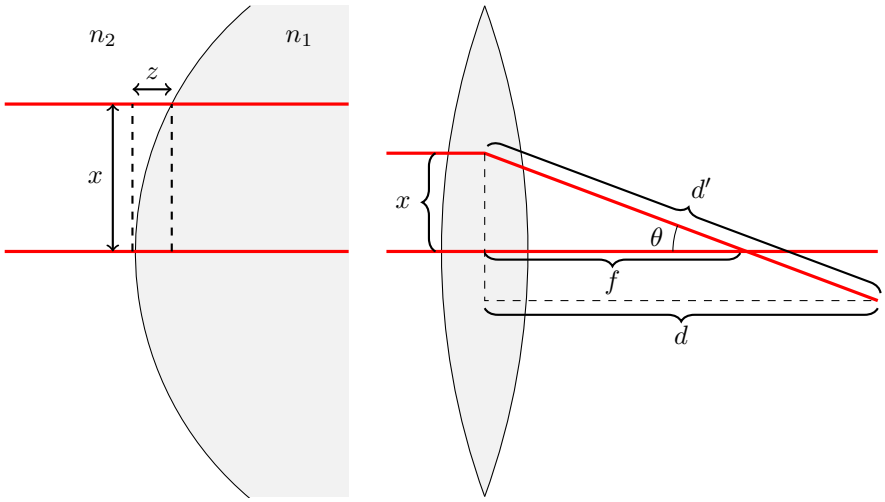

Figure 4: Two possible ways transverse motion of the lenses can cause an optical path difference. On the left, a beam offset from the center of the optic by a distance x travels through the lens a distance z less than a centered beam. On the right, the offset beam is deflected based on the focal length f of the lens. The deflected beam travels a distance d' while the centered beam travels a shorter distance d'.

ment of $x + \delta x$, the beam will travel in the lens z_{tot} less on each side:

$$z_{tot} \approx \frac{x^2}{2R} + \frac{x\delta x}{R} + \frac{(\delta x)^2}{2R} \tag{27}$$

If we consider the beam to be misaligned a fixed distance x off-center and then the beam oscillates with amplitude $\delta x \ll x$ around this point, we will pick up a strain:

$$h = 2(z_{tot} - z)\frac{\Delta n}{L} = 2[x\delta x + (\delta x)^2/2]\frac{\Delta n}{RL} \approx 2x\delta x\frac{\Delta n}{RL} \tag{28}$$

where L is the length of the interferometer and Δn is the difference between the indices of refraction of the lens and of the vacuum. The factor of 2 comes from the fact that the beampath through the lens is shortened on both sides of the lens.

3.2.2 Beam Motion

In order to calculate the noise from variations in the lens thickness, we need to find the initial offset of the beam on the lens. This will be determined by the detector's alignment system. We can assume that the alignment system is able to align the optics so that only 1% of the power inside the arm is lost to higher order modes. From this, we can get an upper bound for the initial misalignment

by calculating the displacement in one lens needed to transfer 1% of the power to the higher order modes if the rest of the system is perfectly aligned. This means that our round trip propagation matrix simplifies to just:

$$P_{rt} = r_1 r_2 t_l^4 P L_1 P^4 L_1 P \tag{29}$$

We can then use Equation 25 to calculate E_{ins} as a function of the transverse displacement of the lens. Here we also assume that E_0 is purely in the TEM_{00} mode. The results of this for the two lens cavity in Figure 2 are plotted in Figure 5. From this plot, we see that $P_{10}/P_{tot} = 0.01$ occurs at 0.81 mm.

From E_{ins}, we can then calculate the transverse displacement of the beam by comparing with the lateral shift operator and the tilt operator, given in Equations 16 and 18. A misalignment of the beam will be a super position of a lateral shift and a tilt. Given a TEM_{00} input beam, he tilt operator gives a purely imaginary coefficient of the TEM_{10} term while the lateral shift operator gives a complex coefficient for the TEM_{10} term which means the real component of a TEM_{10} mode must come from a lateral shift. We can thus calculate the lateral shift Δx_{beam} of the beam at the lens as:

$$\Delta x_{beam} = -w \frac{\mathrm{Re}(E_{10})}{E_{tot}} \tag{30}$$

where w is the beam width at the lens, E_{10} is the TEM_{10} component of the cavity field and E_{tot} is the magnitude of the total cavity field.

What we are interested in is the difference between the beam motion and the lens motion, $\Delta x_{lens} - \Delta x_{beam}$. This relative beam shift is plotted versus Δx_{lens} in Figure 6. We can see from this that our lens motion of 0.81 mm corresponds to a relative off-centering of only 0.11 mm.

3.2.3 Deflection

Taking into account the deflection rigorously is more difficult. However, we can simplify this by considering this noise as a result of the power fluctuation in the cavity field. Shot noise also introduces a power fluctuation in the cavity field and is not a limiting factor at 10 Hz. If we calculate the power fluctuation due to deflection and it is near the same order as the power fluctuation due to shot noise, then we can conclude that the power fluctuation should not be a limiting factor. We can once again consider the cavity to already have an initial misalignment such that there is 1% of the power in the TEM_{10}. We can simply include this misalignment in the input electric field E_0 in Equation 25. We then introduce seismic motion to one of the lenses and calculate the amplitude of the power oscillation in the TEM_{10} mode. This gives the power fluctuation due to deflection P_{def}.

In order to calculate shot noise, we simply use the expression:

$$\Delta P_{shot} = \sqrt{2hcP/\lambda} \tag{31}$$

where h is Planck's constant, c is the speed of light, P is the average power in the electric field, and λ is the wavelength of light[4].

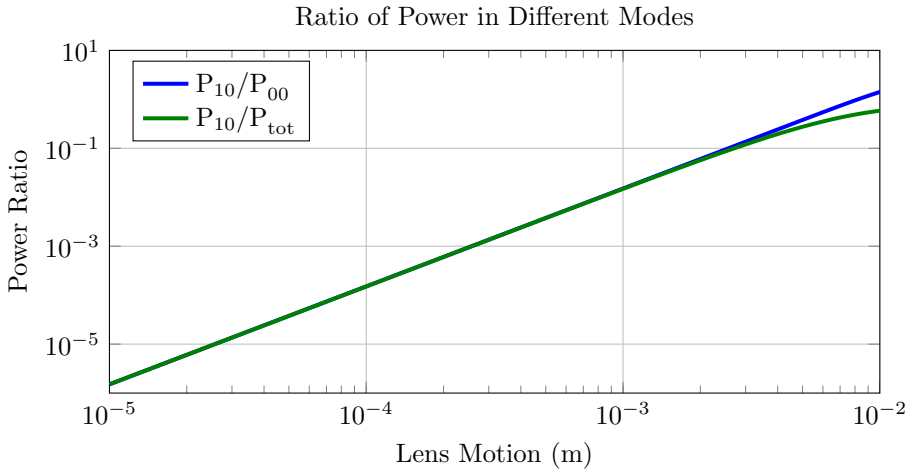

Figure 5: The ratio of power in the TEM_{10} mode compared to the TEM_{00} mode and the overall power as a function of the lens motion. $P_{10}/P_{tot} = 0.01$ at 0.81 mm which we will use as our maximum static misalignment.

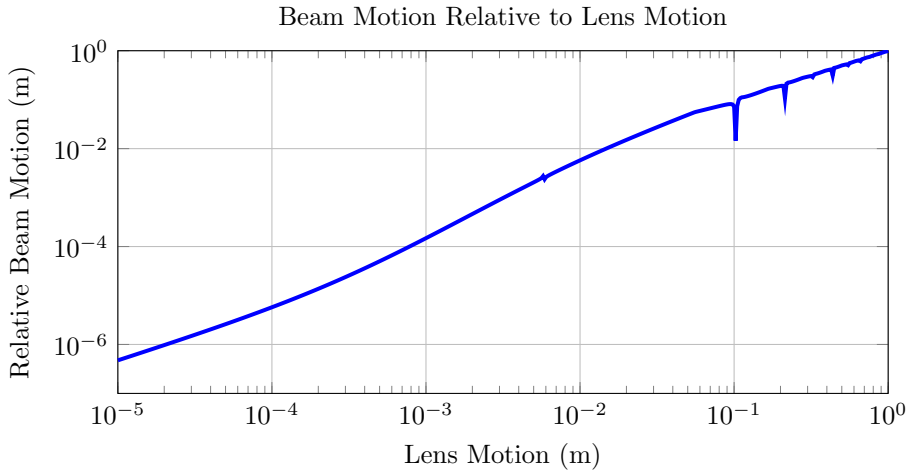

Figure 6: The motion of the beam relative to the center of the lens. For small lens motion, the beam will move roughly in phase with the lens causing the motion of the beam relative to the center of the lens to be even smaller than the lens motion. At a misalignment of 0.81 mm, we see that the beam only moves off-center by 0.11 mm.

3.2.4 Required Seismic Isolation

If the lowest frequency we would like to be sensitive to is 10 Hz, then we require the strain noise here to be less than $10^{-24}\sqrt{\text{Hz}}^{-1}$, 10 times below our desired sensitivity. At 10 Hz the vertical transfer function for a quad suspension without ISI is 3.3×10^{-5} m/m. Based on data from the Livingston detector, we can expect the ground motion to be below 5 nm/$\sqrt{\text{Hz}}$ 95% of the time, leading to a maximum vertical transverse displacement of 1.7×10^{-13} m/$\sqrt{\text{Hz}}$ after applying the quad suspension transfer function[5].

For the two lens cavity we use the 0.11 mm displacement we found above along with the transverse displacement of 1.7×10^{-13} m/$\sqrt{\text{Hz}}$ in Equation 28 to calculate a strain of $3.0 \times 10^{-26}\sqrt{\text{Hz}}^{-1}$ due to the variation in the lens thickness, below our threshold of $10^{-24}\sqrt{\text{Hz}}^{-1}$. For displacement, we calculate the ratio $P_{def}/P_{shot} = 5.9 \times 10^{-4}$, which indicates that the noise introduced through the deflection is much less significant than shot noise. Both noise due to variations in the lens thickness and deflection of the beam are not limiting noise sources for this detector with a quad suspension system with no ISI.

4 Thermal Effects

When a laser beam transmits or reflects off an optic, some of the energy of the beam is transferred to the optic in the form of heat. This heating occurs non-uniformly throughout the optic based on the power distribution of the beam. The power can either be absorbed in the fused silica substrate of the optic or in the anti-reflective (AR) or highly-reflective (HR) coating on the surface of the optic which also affects the temperature distribution. The heating of the optic causes the shape and the index of refraction of the optic to change, both of which effectively change the radius of curvature (or equivalently, the focal length) of the optic. The first phenomenon is known as thermal expansion while the second is known as thermal lensing. While these effects are significant in mirrors, they can be even more pronounced in lenses. In the case of a mirror, very little power transmits into the substrate and mainly only coating absorption occurs. For a lens, nearly the entire power of the beam passes through the substrate and can be absorbed there as well as in the coating. Winkler et al. proposed a simple geometric method to approximate these effects in mirrors[6]. This method only requires slight modifications for lenses.

The method described by Winkler et al. calculates the effects of heating in terms of the effect on the sagitta of the optic. The sagitta is the depth of the optic throughout the beam diameter. Figure 7 shows the definition of the sagitta for a convex lens. While it is clear that thermal expansion will directly affect the sagitta, the effects of thermal lensing create an effective sagitta by altering the optical path length depending on the distance from the center beam.

The sagitta is related to the radius of curvature of the optic by:

$$R \approx \frac{w^2}{2s} \tag{32}$$

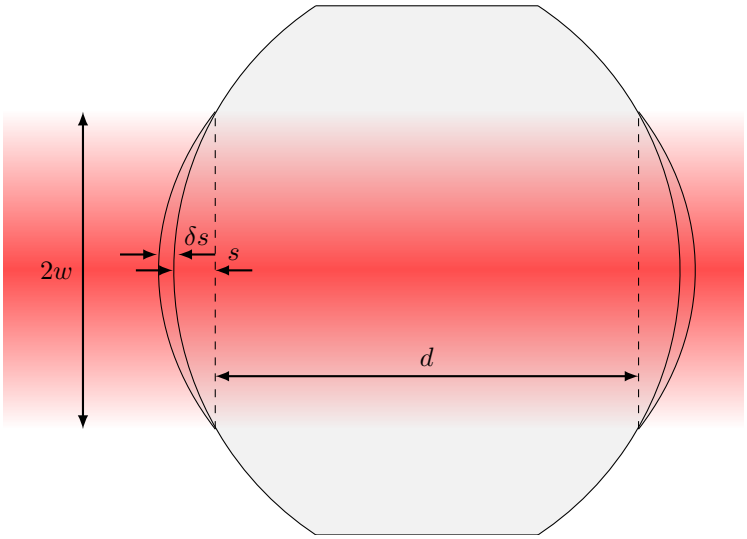

Figure 7: When a laser beam of radius w passes through a lens of thickness d, it deposits heat within a cylinder of length d and radius w. This heat causes the lens to expand, changing the sagitta s of the lens by a small value δs. Additionally, the heat causes the index of refraction of the lens to change, which creates an effective change in the sagitta of the lens.

where R is the radius of curvature, w is the spot size on the optic, and s is the sagitta. The radius of curvature of the lens can then be equated to the focal length f of the lens using the lensmaker's equation. Assuming the lens is biconvex with equal radii of curvature on both sides and sufficiently thin, we see:

$$f = \frac{R}{2(n-1)} = \frac{w^2}{4s(n-1)} \tag{33}$$

where n is the index of refraction of the lens.

Winkler et al. assume the heating takes place in a hemisphere on the surface of the mirror. This is appropriate for heating due to the AR coating on the lenses, but must be modified for heating of the substrate. For coating absorption we will follow Winkler et al. exactly, leading to:

$$\delta s = \frac{(\alpha + \beta) P_a P_{in}}{4\pi\kappa} \tag{34}$$

where δs is the small change in the sagitta, α is the coefficient of thermal expansion of the substrate, $\beta = \frac{dn}{dt}$ is the thermo-optic coefficient of the substrate, P_a is the absorption of the coating, P_{in} is the power incident on the optic, and κ is the heat conductivity of the substrate. Values for these various constants can be found in Table 2. This equation includes both the effects of thermal expansion and thermal lensing.

Parameter	Value	Unit
α	0.51 [7]	$10^{-6}\,\mathrm{K}^{-1}$
β	8.48 [8]	$10^{-6}\,\mathrm{K}^{-1}$
κ	1.38 [7]	W/m·K
n	1.4496 [7]	—
p_a (substrate)	0.15 [9]	ppm/cm
P_a (coating)	1.5 [10]	ppm

Table 2: Thermal properties of the materials of the substrate and lens coating at 20 °C for 1064 nm light. Substrate values are for Suprasil 3001 fused silica except for β which is for Corning 7980 fused silica. AR coating values are for a coating comprised of alternating layers of SiO_2 and Ti doped Ta_2O_5.

In the case of bulk absorption in the substrate, the heating will be distributed throughout a cylinder running through the optic as shown in Figure 7. From Fourier's law, the absorption in the substrate per unit length, p_a, can be equated to a temperature gradient ∇T:

$$p_a P_{in} = \kappa A \nabla T / d \approx 2\pi w \kappa \frac{\delta T}{w} \tag{35}$$

where A is the area of heat transport, w is the spot size, d is the thickness of the lens, and δT is the temperature difference of the optic between the center of the beam and the beam width.

We can also relate the temperature change of the optic with the change in the sagitta δs on each side:

$$\delta s = \frac{\alpha d \delta T}{2} \tag{36}$$

The factor of 2 comes from the fact that this expansion occurs on both sides of the optic.

Comparing these two equations, we can relate δs and P_a:

$$\delta s = \frac{\alpha p_a d P_{in}}{4\pi\kappa} \tag{37}$$

Although the derivation was slightly different, this final result is exactly the same as for the coating thermal expansion except now the absorbed power is dependent on the thickness of the optic.

The thermal lensing effect in the substrate is calculated by Winkler et al. The δs produced by substrate lensing is:

$$\delta s = 1.3 \frac{\beta}{4\pi\kappa} p_a d P_{in} \tag{38}$$

Combining all of these effects, we see that the total change in sagitta is:

$$\delta s = \frac{(\alpha + \beta) P_a + (\alpha + 1.3\beta) p_a d P_{in}}{4\pi\kappa} \tag{39}$$

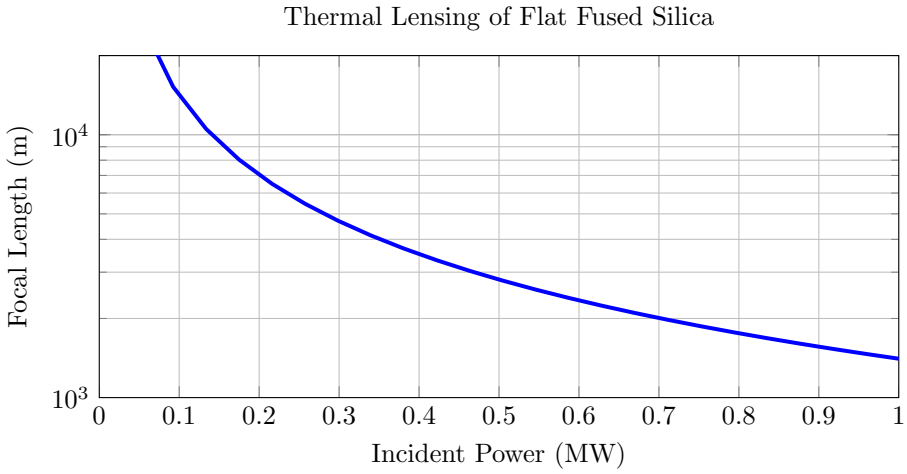

Figure 8: The incident power required on a flat piece of fused silica to achieve a lens of focal length f.

One case we possibility to consider is using flat pieces of fused silica in our detector and relying only on the heating effects to create a lens. A flat piece of fused silica would have no initial sagitta so $s = \delta s$. Using Equations 33 and 39, we can solve for the required incident power P_{in} to create a lens of focal length f:

$$P_{in} = \frac{\pi \kappa w^2}{f(n-1)[(\alpha+\beta)P_a + (\alpha+1.3\beta)p_a d]} \tag{40}$$

Using the thermal properties of fused silica and AR coatings in Table 2 along with the assumptions $d = 10\,\text{cm}$ and $w = 6.7\,\text{cm}$, we arrive at:

$$f \approx \frac{3.17 \times 10^9}{P_{in}} \text{W m} \tag{41}$$

which is plotted in Figure 8. From this, we can see that if our arm cavity uses the same circulating power as aLIGO, approximately 0.8 MW, we will create a lens with a focal length of about 1 km. The most plausible lens configurations include lenses on the order of several km so a thermal compensation system (TCS) will be required to increase the focal length to the desired values. Since the circulating power gives a focal length on the same order as desired, the current TCS system should be powerful enough to create the desired lenses.

5 Conclusions

Our results show that a narrow beam can be transmitted down a 40 km arm with as few as two additional lenses. The noise contribution from the seismic motion of the noises should not be a limiting factor for a 40 km detector if the lenses

are hung from a quadruple pendulum system. Thermal lensing is a significant effect in a long detector and a TCS system will be necessary to decrease the curvature of the lenses.

References

[1] Peter Fritschel and Eric Gustafson. Advanced LIGO H1 optical layout. Technical Report D0902838-v4, LIGO Laboratory, February 2013. URL https://dcc.ligo.org/LIGO-D0902838.

[2] A. E. Siegman. *Lasers*. University Science Books, 1986. ISBN 9780935702118.

[3] Yaron Hefetz, Nergis Mavalvala, and Daniel Sigg. Principles of calculating alignment signals in complex resonant optical interferometers. *J. Opt. Soc. Am. B*, 14(7):1597–1605, Jul 1997. doi: 10.1364/JOSAB.14.001597. URL http://josab.osa.org/abstract.cfm?URI=josab-14-7-1597.

[4] R. Paschotta. Shot noise. In *RP Photonics Encylcopedia*. URL http://www.rp-photonics.com/shot_noise.html.

[5] David J Ottaway, Peter Fritschel, and Samuel J. Waldman. Impact of upconverted scattered light on advanced interferometric gravitational wave detectors. *Opt. Express*, 20(8):8329–8336, Apr 2012. doi: 10.1364/OE.20.008329. URL http://www.opticsexpress.org/abstract.cfm?URI=oe-20-8-8329.

[6] W. Winkler, K. Danzmann, A. Rüdiger, and R. Schilling. Heating by optical absorption and the performance of interferometric gravitational-wave detectors. *Phys. Rev. A*, 44:7022–7036, Dec 1991. doi: 1103/PhysRevA.44.7022. URL http://link.aps.org/doi/10.1103/PhysRevA.44.7022.

[7] *Quartz Glass for Optics: Data and Properties*. Heraeus Quarzglas, July 2014. URL http://heraeus-quarzglas.com/media/webmedia_local/downloads/broschren_mo/DataandProperties_Optics_fusedsilica.pdf.

[8] D. B. Leviton and B. J. Frey. Temperature-dependent absolute refractive index measurements of synthetic fused silica. *ArXiv e-prints*, May 2008.

[9] Laurent Pinard, Daniele Forest, and Raffaele Flaminio. Bulk absorption measurement at 1064 nm of the new Heraeus ultra pure fused silica used for the Advanced Virgo Test Mass: effect of the annealing. Technical Report C1000257, VIRGO, February 2010. URL https://dcc.ligo.org/LIGO-C1000257.

[10] Margot Phelps. Adventures in AR Absorbtion. Presentation at the LVC Collaboration Meeting at Sapienza University, September 2012. URL https://dcc.ligo.org/LIGO-G1200960.